Title
DNA damage modeled with Geant4-DNA: effects of plasmid DNA conformation and experimental conditions

Journal
Physics in Medicine and Biology, 66(24)

ISSN
0031-9155

Authors
D-Kondo, N
Moreno-Barbosa, E
Štěphán, V
et al.

Publication Date
2021-12-21

DOI
10.1088/1361-6560/ac3a22

Peer reviewed

HHS Public Access

Author manuscript

Phys Med Biol. Author manuscript; available in PMC 2022 December 20.

Published in final edited form as:

Phys Med Biol. ; 66(24): . doi:10.1088/1361-6560/ac3a22.

DNA damage modeled with Geant4-DNA: effects of plasmid DNA conformation and experimental conditions

N D-Kondo[1], **E Moreno-Barbosa**[1], **V Štěpán**[2], **K Stefanová**[2], **Y Perrot**[3], **C Villagrasa**[3], **S Incerti**[4], **B De Celis Alonso**[1], **J Schuemann**[5], **B Faddegon**[6], **J Ramos-Méndez**[6,*]

[1]Faculty of Mathematics and Physics Sciences, Benemérita Universidad Autónoma de Puebla, Mexico.

[2]Department of Radiation Dosimetry, Nuclear Physics Institute of the Czech Academy of Sciences, Prague, Czech Republic.

[3]Laboratoire de Dosimétrie des Rayonnements Ionisants, Institut de Radioprotection et Sûreté Nucléaire, Fontenay aux Roses, BP. 17, 92262, France

[4]Univ. Bordeaux, CNRS/IN2P3, CENBG, UMR 5797, F-33170 Gradignan, France.

[5]Physics Division, Department of Radiation Oncology, Massachusetts General Hospital & Harvard Medical School, Boston, MA, USA.

[6]University of California San Francisco Comprehensive Cancer Center, San Francisco, California, USA.

Abstract

The chemical stage of the Monte Carlo track-structure code Geant4-DNA was extended for its use in DNA strand break (SB) simulations and compared against published experimental data. Geant4-DNA simulations were performed using pUC19 plasmids (2686 base pairs) in a buffered solution of DMSO irradiated by ^{60}Co or ^{137}Cs γ-rays. A comprehensive evaluation of SSB yields was performed considering DMSO, DNA concentration, dose and plasmid supercoiling. The latter was measured using the super helix density value used in a Brownian Dynamics (BD) plasmid generation algorithm. The Geant4-DNA implementation of the Independent Reaction Times method (IRT) developed to simulate the reaction kinetics of radiochemical species, allowed to score the fraction of supercoiled, relaxed and linearized plasmid fractions as a function of the absorbed dose.

The percentage of the number of strand breaks after •OH + DNA and H• + DNA reactions, referred as SSB efficiency, obtained using MCTS were 13.77% and 0.74% respectively. This is in reasonable agreement with published values of 12% and 0.8%. The SSB yields as a function of DMSO concentration, DNA concentration and super helix density recreated the expected published experimental behaviors within 5%, one standard deviation. The dose response of SSB and DSB yields agreed with published measurements within 5%, one standard deviation.

We demonstrated that the developed extension of IRT in Geant4-DNA, facilitated the reproduction of experimental conditions. Furthermore, its calculations were strongly in agreement with

*Corresponding author.

experimental data. These two facts will facilitate the use of this extension in future radiobiological applications, aiding the study of DNA damage mechanisms with a high level of detail.

1. Introduction

Monte Carlo Track Structure (MCTS) codes have allowed us to deepen our understanding of radiation damage in biological tissue. MCTS codes provide detailed information of each and every interaction of an energetic ionizing particle with matter along the particle track. A list of MCTS codes and past works on DNA damage modeling was published along the last decades, see e.g., Berger et. al.(1973), Booz et. al.(1988), Chatterjee et. al.(1985), Friedland et. al. (2002), Leenhouts et. al.(1985), Nikjoo et. al. (1998). Toburen (2014), Turner et. al. (1983), Wright et. al. (1985), Zaider et al. (1983). Radiation damage to biological tissue has been associated with the breakage of cellular DNA caused by either direct or indirect action. In the direct action, the damage is caused by energy transfer to DNA molecules, whereas in indirect action, the creation of reactive chemical species by radiolysis of the medium in close proximity to the DNA induces the damage by reacting with the DNA molecule (Hall & Giaccia, 2012). Simulation with MCTS has historically allowed for detailed studies of the interaction of ionizing radiation with biological structures such as DNA damage through the direct and indirect pathways.

The Geant4-DNA project (Bernal et al., 2015; Incerti et al., 2010; Incerti et al., 2010; Incerti et al., 2018) extended the Geant4 toolkit to include track structure capabilities in 2010. More recently, Geant4-DNA added radiation chemistry models to simulate all stages of water radiolysis including the physical, pre-chemical and chemical stages. For the physical and pre-chemical stages, a comprehensive description of the processes and models available in Geant4-DNA has been given elsewhere Karamitros et al. (2011, 2014), Incerti et al. (2018), Shin et al. (2021). For the chemical stage, two methods were provided; one based on the Step-By-Step approach (Karamitros et al., 2011, 2014), the other based on the Independent Reaction Times (IRT) approach (Clifford et. al., 1986; Greenet. al1990; Pimblott et. al, 1992; Ramos-Méndez et al., 2020) Geant4-DNA has been used widely for DNA damage simulations. Applications included the simulation of a fibroblast cell nucleus irradiated with protons (Meylan et al., 2017), chromatin fibers irradiated with protons and alpha particles (de la Fuente et al., 2018), a bacterial cell irradiated with electrons and protons (Lampe et al., 2018), a fractal cell nucleus irradiated with protons (Sakata et al., 2019) and straight DNA segments irradiated with electrons (Lampe et al., 2018). In these works, direct and indirect contributions to the DNA damage in complex structures were simulated. In all cases, Geant4-DNA reproduced the trend of the experimental results as a function of the particle linear energy transfer (LET). However, the use of such complex geometries had the disadvantage of demanding longer times (hours to days) to prepare the geometry for irradiation together with the particle source. In addition, experimental procedures to measure DNA breakage in cells has proven to be a complicated process with multiple techniques available (Figueroa-González & Pérez-Plasencia, 2017) not providing the sufficient spatial resolution to directly compare calculated to measured DNA breakage. For instance, in most cases, the presence of repair proteins is used as a site marker providing an indirect method to estimate DNA damage.

However, MCTS accuracy for DNA damage estimation can be questioned, with SSB efficiencies ranging from 25% to 65% (Lampe et. al., 2018; Meylan et. al. 2017; Tomita et. al., 1998; Friedland et. al., 2011) compared with the experimental results of 12% (Milligan et. al., 1993). This could lead to an over estimation not only of SSBs, but also of more complex break types that depend on SBs distributions. With the recent improvements to the physical and chemical models of Geant4-DNA/TOPAS-nBio (Shin et. al., 2021; Ramos-Mendez et. al., 2020), which have been observed to have a great impact on •OH and e_{aq}^{-}, with differences around 35% and 22% were observed at 1μs (Peukert et. al., 2019). Therefore, a decrease in DNA SBs is expected, which is of particular interest to the radiation chemistry area moving forward into temperature and oxygen depletion effects on DNA SBs.

In this work, the IRT approach implemented in Geant4-DNA was benchmarked for its use in predicting plasmid DNA damage response in experimental conditions. This was achieved with a less complex geometrical approach than a cell nucleus consisting of plasmids pUC19 (2686 base pairs) irradiated by low LET radiation. Due to their relatively low number of base pairs compared with DNA contained in a cell nucleus (2–6 Gbps), plasmids were easier to manage computationally than cellular DNA. Experimentally, their trademark “supercoiling” property allowed scientists to identify strand breaks experimentally and classify them as a SSB or a DSB (Casali & Preston, 2003; Hempel & Mildenberger, 1987; Higgins & Vologodskii, 2015). The plasmid supercoiling property was measured by the super helix density. A super helix density different than zero meant that the DNA was under stress creating higher order helix geometries (Vologodskii & Nicholas, 1994). The use of computational plasmid models allowed us to efficiently compare different scenarios of DNA damage response. The investigated scenarios included the comparison with published measured data of SSB yields as a function of DNA concentration, scavenger concentration and plasmid superhelix density (σ). In addition, comparison of calculated SSB and DSB yields as a function of the absorbed dose with published data was performed.

2. Methodology

A Geant4-DNA application using the IRT method was developed to model radiation damage in supercoiled plasmid DNA. The application used the low energy physical models available in the “G4EmDNAPhysics_option2” physics list and the chemical processes modeled by the IRT provided by Geant4-DNA version 10.7.p01 (Ramos-Méndez et al., 2020). The application facilitated the control of the radiation source, loading of plasmid data files, the number of plasmids geometries and radiation chemistry conditions.

2.1. Chemical stage simulation

The IRT implementation of Geant4-DNA includes more than 70 reactions to help model radiation chemistry processes (Ramos-Méndez et al., 2020). The heterogenous chemistry process that follow water radiolysis, has been successfully simulated using a reduced number of chemical reactions (Pimblott & LaVerne, 1997; Ramos-Méndez et al., 2018; Shin et al., 2019). Reactions used with the IRT in this work are presented in Table 1. The use of a reduced number of chemical reactions was done in order to decrease simulation times as much as possible while maintaining precision.

Experimental irradiation conditions of DNA plasmids included a cryopreservative which acted as a scavenger for •OH, thus protecting the DNA from damage after irradiation, e.g., dimethyl sulfoxide (DMSO), tris(hydroxymethyl)aminomethane (TRIS) or ethylenediaminetetraacetic acid (EDTA). The presence of cryopreservatives was modeled by first-order reactions considering their scavenging capacity. The reactions involving such scavengers also occurred at longer times (around 10 μs for 10^{-4} M DMSO) than the heterogeneous chemistry stage (1μs). Thus, classes in Geant4-DNA dealing with the IRT method were modified to allow reactions between chemical species and buffered solutions until 20 μs. Reactions with dissolved O_2 were also considered to recreate experimental aerobic conditions (Milligan et al., 1992, 1993, 1996; Tomita et al., 1995, 1998) and these were obtained from (Buxton et al., 1988), see Table 1. In reactions 11, 12, and 13, DNA referred to a deoxyribose-phosphate pair center. This was done to reduce the number of chemical species in the IRT, reducing computing time.

The reaction rate coefficient of reaction 11, k_{11} ($M^{-1}s^{-1}$), was measured by Milligan et al.(1996), and is shown in equation 1 as a function of •OH scavenging capacity, s:

$$k_{11} = 1.32 \times 10^{7} s^{0.29} \quad (1)$$

2.2. DNA Model: pUC19 Plasmids

In this work, plasmid "skeletons" for pUC19 were generated using a Brownian Dynamic (BD) approach (Ermak & McCammon, 1978; Huang et. al., 2001). Starting from an open circle composed of n evenly spaced vertexes and slowly deforming the configuration until a total simulation time of 5 μs was achieved. The main parameters for the plasmid generation algorithm were temperature, super helix density, and number of vertexes (Vologodskii & Cozzarelli, 1994). Plasmid super helix density is a measure of plasmid supercoiling. It is the ratio between the difference in the number of turns of the DNA helix in a relaxed state and the actual number of turns divided by the number of turns in a relaxed state (Vologodskii & Cozzarelli, 1994). This difference causes an energy change that plasmid generation algorithms use to perform small plasmid vertex displacements. The temperature and super helix density were used to compute the total energy of the configuration, which affects the grade of supercoiling of the plasmid. While the number of vertexes corresponds to the length of the plasmid and as so, the type of plasmid (pUC19, pB322, pVC40, etc). The initial parameters were 20 °C and a superhelix density (σ) ranging from −0.06 to −0.03 and 2686 vertexes. In total, a set of 40 pUC19 plasmids were generated, 10 for each σ value: −0.03, −0.04, −0.05 and −0.06 (Figure 1a). The mean writhe of these plasmids were: −11.83 ± 0.37, −9.94 ± 0.46, −7.85 ± 0.45, and −5.92 ± 0.51, respectively, calculated with the Gaussian integration method reported by (Klenin & Langowski, 2000).

A basic DNA model consisting of semi-spheres was used to wrap the plasmid skeleton as shown in Figure 1b. The 2686 base pairs of pUC19 were accommodated in a deformed polygon of 179 straight sides of the same length. Each side contained 14 to 15 base pairs accommodated to avoid overlapping. The number of straights sides and base pairs could be changed by the user. However, we found that between 10 and 20 base pairs (3.4 to 6.8 nm) produced a reasonably well behaved figure. The spatial and angular separations between two

base pairs were 0.34 nm and 36°, respectively. Each base pair was modeled using six cut spheres, two for the nucleobases, two for the deoxyriboses and two for the phosphates. The radii were 2.45 Å, 2.93 Å, and 2.7 Å, respectively. These values were obtained to achieve the same geometric volume as that provided by the DNAfabric software previously reported in (Meylan et. al., 2016).

2.3. DNA damage efficiency.

Due to different reaction pathways, not all hydrogen atom abstractions involved in the reaction between $^{\bullet}OH$ and $H^{\bullet}$ with DNA produced an indirect Strand Break (SB) (Dizdaroglu & Jaruga, 2012). Thus, for modeling purposes an indirect SB is produced with an efficiency given by a probability λ, after one reaction between $^{\bullet}OH$ or $H^{\bullet}$ with DNA occurred. In this work, we calibrated the indirect SB efficiency by using a Nelder-Mead (NM) optimization algorithm (Nelder & Mead, 1965). We compared the simulation results with experimental data and minimized their difference using a two-parameter method shown by the following function:

$$F(\lambda_{OH}, \lambda_H) = \int_{x_i}^{x_f} \left| y_{reff}(x) - (\lambda_{OH} OHDNA(x) + \lambda_H HDNA(x)) \right| dx \quad (2)$$

where y_{reff} was the measured reference data, OHDNA and HDNA the yields of the products from reactions 11 and 12, respectively, while the integration limits xi and xf are dependent on the specific simulation setup. The fitted parameters λ_{OH} and λ_H, were the SB efficiencies for $^{\bullet}OH$ and $H^{\bullet}$, respectively. Initial values of λ_{OH} and λ_H were randomly taken from 0 to 1 and 0 to 0.1, respectively, with neither value allowed to be below 0 or above 1 during the NM procedure. The NM algorithm was conducted until the difference between the best and worst value of $F(\lambda_{OH}, \lambda_H)$ converged within 0.1%. The NM procedure was repeated 100 times with different random number seeds and the results were used to obtain the mean and standard deviation of the SB efficiencies. This was done to mitigate the effect of the algorithm finding a local minimum instead of the global minimum. This calibration procedure was applied to scenario S1 (Table 2) and the obtained SB efficiencies were used for the remaining scenarios.

2.4. Strand Break Scoring

A direct SB was registered if at least 17.5 eV was accumulated in the sugar and phosphate volumes on one side of a single base pair (Charlton et. al., 1989; Lampe et. al., 2018). For indirect SB, we performed the following.

1. Each individual base pair (nucleotide, phosphate and deoxyribose) was taken as one whole chemical species or molecule and inputted into the IRT, with its position being centered between the sugar-phosphate volumes. This was done based on the use of observed reaction rate constants between chemical species and DNA (Perry et. al., 2020; H. Tomita et al., 1998).
2. OHDNA and HDNA yields were converted to SB yields by using the relationship $SB = OHDNA \cdot \lambda_{OH} + HDNA \cdot \lambda_H$.

3. SB were accumulated and classified as SSBs and DSBs in order to be compared with experimental data. In this regard, we defined one DSB as two SSBs located on opposite strands with a distance of 10 base pairs or less.

Cell survival fraction is attributed to complex DNA strand breaks like the ones studied in (Charlton et al., 1989; Georgakilas et. al., 2013; Watanabe et. al.,, 2015). However, due to the lack of experimental resolution, these high complexity breaks are hard to measure. Most plasmid experimental results on the other hand are presented using only SSBs and DSBs by making use of the loss of super coiling and DNA linearization fractions (Edel et. al., 2006; Vyšín et al., 2015) and do not include DNA repair processes. In this validation work, Geant4-DNA simulations were compared against different experimental results by using the SSBs and DSBs yields, without considering the repair kinetics. However, Geant4-DNA has been successfully used alongside DNA repair models (Sakata et. al., 2020).

Given the presence of a geometrical model like bound DNA volumes (filled with water for all simulations), we considered two scenarios involving the origin of primary chemical species. In the first scenario (A1) only chemical species created outside of the DNA volumes were inputted into the IRT. Species created inside the DNA were discarded without contributing to the chemistry. For the second scenario (A2), the simulation included both, species created inside and outside of the DNA volumes into the IRT. A2 was conducted only to serve as a comparison with A1 as inside the DNA volumes there should not be any free water molecules to be dissociated.

2.5. Simulation Setup

Four different setups were used to compare simulation results with experimental data. All setups shared the same geometry consisting of a 1 μm diameter water sphere (ρ=1 g/cm^3) containing up to 20 plasmids positioned uniformly (Figure 1b), as well as the same oxygen concentration ([O_2]) of 0.27 mM. One pUC19 plasmid in the sphere was equivalent to a concentration of 5.62 μg/mL DNA. Simulation scenarios were configured to recreate the experimental conditions from their respective references (Table 2). Scenario S1 was conducted using 30 Gy of dose with a [DNA] of 50.6 μg/mL, [DMSO] ranged from 10^{-4} to 1 M and the plasmids super helix density was −0.03. Scenario S2 configuration used 30 Gy of dose with [DNA] ranging from 5.62 – 100.12 μg/mL, [DMSO] of 10^{-3} M and plasmids super helix density of −0.03. Scenario S3 was conducted using 80 Gy of dose, 50.6 μg/mL of [DNA], 4.56 ×10^{-3} M of [DMSO], plasmids super helix density ranged from −0.06 to −0.03. Scenario S4 used a dose ranging from 0 – 120 Gy, 33.73 μg/mL of [DNA], 2.28 ×10^{-4} M of [DMSO] and plasmid super helix density of −0.03. Scenarios S1, S2 and S3 shared the same ^{137}Cs source, while S4 used a ^{60}Co source following their experimental conditions.

Results from scenarios S1, S2, and S3 were compared with data from Milligan et al., (1993, 1992, 1996). Results from scenario S4 were compared with data from Tomita et al., (Tomita et al., 1998; Tomita et al., 1995). In Tomita et al., the authors used pBR322 (4362 bps) plasmids at a concentration of 30 μg/mL and the •OH scavenging capacity of the environment was 1.62×10^6 s^{-1} (0.1 Tris EDTA buffer). Thus, the concentration of DMSO for scenario S4 was calculated to match the •OH scavenging capacity used by Tomita in

order to allow the comparison. The reaction kinetics of the products from reactions with scavengers was not considered in this work. Simulations were repeated using different random seeds; 100 times for scenarios S1, S2 and S4, and 24 times for S3. From the results, the mean yields and standard deviations were calculated. In all the scenarios, the energy deposited by particle tracks was accumulated in the water sphere until an absorbed dose was achieved. We considered that each individual track was independent from any the other.

Due to the low interaction probability of γ-rays in such a small volume (1 μm), the spectrum of secondary electrons produced by ^{60}Co or ^{137}Cs γ-rays interacting in water (neglecting pair production) was obtained to increase computational efficiency (Figure 2). For that, each spectrum was calculated in a separated simulation using condensed history Monte Carlo with TOPAS (Perl, et. al., 2012). A γ-ray point source was positioned at the center of a spherical water phantom of 5 cm radius. The source was isotropic, emitting γ-rays of 0.662 MeV for ^{137}Cs, or two γ-rays of 1.33 MeV and 1.17 MeV for ^{60}Co. The spectrum of initial kinetic energy (at the point of energy transfer) of the secondary electrons produced by γ-rays was scored at 5–5.2 cm depth in water to account for photon scatter.

For the SSB and DSB simulations (scenarios S1 to S4), the electron source was isotropic and uniformly distributed in the spherical water phantom of 1 μm diameter. The initial electron energy was sampled from the appropriate spectrum (^{137}Cs or ^{60}Co).

3. Results

The calculated yield of SSB, G(SSB), as a function of the DMSO concentration (scenario S1) is shown in Figure 3 for setup A1, see section (2.4). The values λ_{OH} of 13.77% ± 0.64% and λ_H of 0.74% ± 0.07% were obtained with the minimization algorithm. The results obtained agreed with the experimental measurements within one standard deviation. For setup A2 which included radiolitic species created in all regions of the simulation setup (see section 2.3), the resulted efficiency is 23.77%. Subsequent results in this work use the 13.77% efficiency value.

The calculated dependence of SSB yield on DNA concentration (scenario S2) is shown in Figure 4. Results show reasonable agreement within the statistical uncertainties. The mean statistical uncertainty of the simulation results was 2.4%. Simulation agrees with measured data with a slope difference of 4.47 ± 2.3%.

The G(SSB) response to superhelix density obtained in scenario S3 is presented in Figure 5. Simulation results are shown alongside experimental data.A reasonable agreement was achieved between simulation and experimental measurements within one standard deviation. Simulation mean statistical uncertainties were of 4.6%. Simulation results were obtained by considering correction factors from Milligan et. al. (1992). These correction factors account for the ethidium binding to supercoiled DNA, not simulated, which goes from 3.3 at 0 σ to 1.1 at −0.08 σ. Hence, a half-point value for ethidium correction of 2.2 was used resulting in satisfactory agreement with the measured data.

Results for DNA damage as a function of absorbed dose (scenario S4) are shown in figure 6. Both SSB and DSB agreed with experimental data within statistical uncertainties with differences of 5.84% and 14% for SSB and DSB respectively.

The curves of plasmid fraction are shown in Figure 7. Calculated results were fitted using the Cowan model (Cowan et. al., 1987). Fitting parameters for the Cowan model resulted in $\mu = 2.92\times10^{-2}$ SSB Plasmid^{-1} Gy^{-1} and $\Phi = 4.45\times10^{-4}$ DSB Plasmid^{-1} Gy^{-}1. For the fitting procedure, it was assumed that no strand break yields were produced at zero doses ($\mu_0 = 0$ and $\Phi_0 = 0$).

Direct DNA damage results for different DNA concentrations are shown in Table 3. These results were obtained with 50,000 source electrons interacting in the 1 micrometer diameter sphere.

4. Discussion

In this work we extended and benchmarked the Geant4-DNA IRT implementation for its use as a DNA SSB and DSB prediction tool. An overall good agreement was achieved for all simulated scenarios, recreating the trend of published experimental results within one standard deviation. The results were applicable to low LET regimes while only considering radiolitic species created outside of the DNA volumes (setup A1).

For the simulation scenario S1, DNA damage efficiencies exceed experimental values of 12% for $^{\bullet}$OH (versus 13.77 ± 0.64% from our simulations) as reported by Milligan et al., (1993) and 0.8% for H$^{\bullet}$ (versus 0.74 ± 0.07%) obtained by Aydogan et. al. (2008). For $^{\bullet}$OH yields calculated in liquid water with the IRT implemented in Geant4-DNA (Ramos-Méndez et al., 2020, 2018), an exceess in the G value $^{\bullet}$OH radicals of about 10% exists at around 1 ns, around the time corresponding to the scavenging capacities used in this work. By reducing the $^{\bullet}$OH yields discrepancies, we expect an increase of up to 10% in SB efficiency, which will give us 23.77%, well in excess of 12%. The DNA geometry model might assist in resolving that issue having an impact on SB yields. For example, a 10% difference in SB yields was found when comparing A2 with A1. This difference is based purely on DNA geometry volumes. Hence, by using more detailed DNA models, it is possible to compensate the increase in SB efficiencies due to $^{\bullet}$OH yields once the chemical models are updated, maintaining a good agreement with the experimental value of 12%. Thus, reducing the DNA geometry dimensions might compensate the excess in efficiency. This can be explained as follows. By accepting chemical species produced in the DNA volumes, the chance of reactions at the contact with DNA molecules increased and hence increased the number of SB. The study corresponding to the DNA geometry dimension is a subject of a future work.

Scenario S2 recreated the behavior of the measured SSB yields as a function of the DNA concentration within one standard deviation. Slope values differ slightly with 4.47 ± 2.3%. Simulated results tend to diverge from the fitted experimental data results as concentration of DNA increases; with an initial difference of 4.07% at 5.62 μg/mL and 8.04% at 101.19 μg/mL. However, since this fit is only taking into account the reported values

without considering statistical errors from those, we can assume a reasonable agreement for concentration of DNA response of SSB yields.

Both experimental and simulated results for scenario S3 showed a trend of monotonic increasing SSB yield with increasing superhelix density. This could be explained by a "protective" effect caused by the DNA volume (Takata et al., 2013). In other words, due to the larger region of condensed DNA where chemical species cannot be created, the separation distance between inner DNA and chemical species increased, reducing the likelihood of reaction. The increase from −0.06 to −0.03 accounts for a difference of 4.5%, which suggest that the more packed the DNA is, the less likely it is to break, as mentioned by Takata (2013). However, these effects in plasmids are not as accentuated as with chromatin fibers in which the SB yield can go up to 50 times between condensed and decondensed chromatin.

For scenario S4, simulated SSB yields had a linear response and eventually reach curvature towards 120 Gy. Although it was reported that SSB should behave linearly at low doses (Klimczak et. al., 1993; Tomita et al. 1998), non-linear behavior of SSB at high doses had also been observed experimentally (Kassis et. al. 1999b, 1999a). As shown by Kassis et. al., SSBs exhibited a threshold of dose (around 30 Gy in absence of DMSO) after which it reached a plateau and remained constant. However, DSBs continued to increase nonlinearly. This suggested that as SSBs continued being produced with the dose increase, these also were being created closer leading to more DSBs. Such behavior was accelerated as DMSO decreased (as shown in Figure 8). That behavior was consistent with data from Kassis et al. These effects are expected to be seen in the scenario of high doses in cellular scavenging conditions (equivalent to around 0.1 to 1 M [DMSO]). Thus Geant4-DNA was capable of reproducing that behavior satisfactorily.

By using the results from scenario S4, we provided a means to obtain curves of plasmid fraction response to dose. The obtained results behave consistently with published data. For instance, Vyšín et al., (2015) reported plasmid fraction response curves for 20 MeV protons. They obtained parameters for SSB and DSB per plasmid and Gy of 3.27×10^{-1} and 1.26×10^{-2} whereas we obtained 2.92×10^{-2} and 4.45×10^{-4}. The observed difference may be attributed to the difference in LET from ≈ 5.0 keV/μm to 0.3 keV/μm for 20 MeV protons, and ^{60}Co γ-ray, respectively.

The contribution of SSB produced by direct action under low LET radiation conditions (< 0.91 keV/um) (Meesungnoen, Benrahmoune, Filali-Mouhim, Mankhetkorn, & Jay-Gerin, 2001)) was expected to be low (Klimczak et al., 1993; Vyšín et al., 2015). The calculated total direct contribution was less than 0.01%, whereas the experimental value measured by Tomita et al. (1995) for indirect DNA damage contribution was 98.5 ± 2.5% (1.5 ± 2.5% direct DNA damage contribution). The differences in contribution values fell within the experimental uncertainty. The result also depends on the size of the spherical components of the DNA plasmid and the contribution of very low energy electrons. Gao et al (2021), showed that low energy electrons irradiating iced plasmids produced considerable DNA damage (4.86 – 160 SSB μmol J^{-1}). This data might provide an improved benchmark which is subject of a future work.

5. Conclusions

In this work the IRT approach implemented in Geant4-DNA was succesfully modified to simulate DNA strand breaks and water radiolisis simulations at times greater than 1 μs. The algorithm was benchmarked for its use in estimating SSB and DSB in pUC19 plasmids using low LET radiation using both ^{60}Co and ^{137}Cs equivalent sources. We achieved agreement between simulated results and experimental data for all simulated scenarios within one standard deviation of SSB and DSB yields. The obtanied SSB efficiency values were close to experimental results, albeit outside of experimental uncertainty for $^{\bullet}$OH. This Geant4-DNA application will soon be incorporated as part of the Geant4 examples and can then be used as a reliable tool to calculate SSB and DSB in plasmids. This application may also be used in a future work to test higher LET regimes by using heavy ions.

Acknowledgements

This work is part of D-Kondo N. doctoral studies from the “Programa de Doctorado en Ciencias Fisica Aplicada, Benemerita Universidad Autonoma de Puebla” Mexico. The first author received financial support for his studies from fellowship 2019-000002-01NACF-05024 from CONACYT, México. Ramos-Méndez J.,Schuemann J. and Faddegon B. were supported by the NIH/NCI R01 CA187003 (TOPAS-nBio) grant. To Wook-Geun Shin from Department of Radiation Oncology, Seoul National University Hospital, Seoul 03080, Republic of Korea for his contribution in the development of Geant4-DNA IRT. All the simulation work was made with the support of the computer resources provided by the Laboratorio Nacional de Supercómputo del Sureste de México trough grant number 202001012C.

References

Aydogan B, Bolch WE, Swarts SG, Turner JE, & Marshall DT (2008). Monte Carlo simulations of site-specific radical attack to DNA bases. Radiation Research, 169(2), 223–231. 10.1667/RR0293.1 [PubMed: 18220458]

Berger MJ, Seltzer SM (1973). ETRAN, Monte Carlo code system for electron and photon transport through extended media. Retrieved from https://rsicc.ornl.gov/PackageDetail.aspx?p=ETRAN&id=C00107&cpu=I0360&v=00&t=Monte Carlo Code System for Electron and Photon Through Extended Media.

Bernal MA, Bordage MC, Brown JMC, Davídková M, Delage E, El Bitar Z, … Incerti S (2015). Track structure modeling in liquid water: A review of the Geant4-DNA very low energy extension of the Geant4 Monte Carlo simulation toolkit. Physica Medica, 31(8), 861–874. 10.1016/j.ejmp.2015.10.087 [PubMed: 26653251]

Booz J, & Feinendegen LE (1988). A microdosimetric understanding of low-dose radiation effects. International Journal of Radiation Biology, 53(1), 13–21. 10.1080/09553008814550381

Buxton GV, Greenstock CL, Helman WP, & Ross AB (1988). Critical Review of rate constants for reactions of hydrated electrons, hydrogen atoms and hydroxyl radicals (·OH/·O− in Aqueous Solution. Journal of Physical and Chemical Reference Data, 17(2), 513–886. 10.1063/1.555805

Casali N, & Preston A (2003). E.coli Plasmid Vectors. Methods in molecular biology (Vol. 253). Totowa, New Jersey: Humana Press. 10.1007/978-1-60761-820-1_12

Charlton DE, Nikjoo H, & Humm JL (1989). Calculation of Initial Yields of Single-Strand and Double-Strand Breaks in Cell-Nuclei From Electrons, Protons and Alpha-Particles. International Journal of Radiation Biology, 56(1), 1–19. 10.1080/09553008914551141 [PubMed: 2569005]

Chatterjee A, & Magee JL (1985). Theoretical Investigation of the Production of Strand Breaks in DNA by Water Radicals. Radiation Protection Dosimetry, 13(1–4), 137–140.

Clifford P, Green NJB, Oldfield MJ, Pilling MJ, & Pimblott SM (1986). Stochastic models of multi-species kinetics in radiation-induced spurs. Journal of the Chemical Society, Faraday Transactions 1: Physical Chemistry in Condensed Phases, 82(9), 2673–2689. 10.1039/F19868202673

Cobut V, Frongillo Y, Patau JP, Goulet T, Fraser MJ, & Jay-Gerin JP (1998). Monte Carlo simulation of fast electron and proton tracks in liquid water - I. Physical and physicochemical aspects. Radiation Physics and Chemistry, 51(3), 229–243. 10.1016/S0969-806X(97)00096-0

Cowan R, Collis CM, & Grigg GW (1987). Breakage of double-stranded DNA due to single-stranded nicking. Journal of Theoretical Biology, 127(2), 229–245. 10.1016/S0022-5193(87)80133-9 [PubMed: 2826926]

de la Fuente Rosales L, Incerti S, Francis Z, & Bernal MA (2018). Accounting for radiation-induced indirect damage on DNA with the Geant 4-DNA code. Physica Medica, 51(June), 108–116. 10.1016/j.ejmp.2018.06.006 [PubMed: 29908994]

Dizdaroglu M, & Jaruga P (2012). Mechanisms of free radical-induced damage to DNA. Free Radical Research, 46(4), 382–419. 10.3109/10715762.2011.653969 [PubMed: 22276778]

Edel S, Terrissol M, Peudon A, Kümmerle E, & Pomplun E (2006). Computer simulation of strand break yields in plasmid pBR322: DNA damage following 125I decay. Radiation Protection Dosimetry, 122(1–4), 136–140. 10.1093/rpd/ncl453 [PubMed: 17185311]

Ermak DL, & McCammon JA (1978). Brownian dynamics with hydrodynamic interactions. The Journal of Chemical Physics, 69(4), 1352–1360. 10.1063/1.436761

Figueroa-González G, & Pérez-Plasencia C (2017). Strategies for the evaluation of DNA damage and repair mechanisms in cancer. Oncology Letters, 13(6), 3982–3988. 10.3892/ol.2017.6002 [PubMed: 28588692]

Friedland W, Bernhardt P, Jacob P, Paretzke HG, Dingfelder M, Cherubini R, … Ottolenghi A (2002). Simulation of DNA damage after proton and low let irradiation. Radiation Protection Dosimetry, 99(1–4), 99–102. 10.1093/oxfordjournals.rpd.a006848 [PubMed: 12194370]

Friedland Werner, Dingfelder M, Kundrát P, & Jacob P (2011). Track structures, DNA targets and radiation effects in the biophysical Monte Carlo simulation code PARTRAC. Mutation Research - Fundamental and Molecular Mechanisms of Mutagenesis, 711(1–2), 28–40. 10.1016/j.mrfmmm.2011.01.003 [PubMed: 21281649]

Gao Y, Zheng Y, Sanche L. Low-Energy Electron Damage to Condensed-Phase DNA and Its Constituents. International Journal of Molecular Sciences. 2021; 22(15):7879. 10.3390/ijms22157879 [PubMed: 34360644]

Georgakilas AG, O'Neill P, & Stewart RD (2013). Induction and repair of clustered DNA lesions: What do we know so far? Radiation Research, 180(1), 100–109. 10.1667/RR3041.1 [PubMed: 23682596]

Green NJB, Pilling MJ, Pimblott SM, & Clifford P (1990). Stochastic modeling of fast kinetics in a radiation track. Journal of Physical Chemistry, 94(1), 251–258. 10.1021/j100364a041

Hall EJ, & Giaccia AJ (2012). Radiobiology for the radiologist: Seventh edition. Radiobiology for the Radiologist: Seventh Edition (7th ed.).

Hart EJ, & Boag JW (1962). Absorption Spectrum of the Hydrated Electron in Water and in Aqueous Solutions. Journal of the American Chemical Society, 84(21), 4090–4095. 10.1021/ja00880a025

Hempel K, & Mildenberger E (1987). Determination of g-values for single and double Strand break induction in plasmid DNA using agarose gel electrophoresis and a curve-fitting procedure. International Journal of Radiation Biology, 52(1), 125–138. 10.1080/09553008714551551

Huang J, Schlick T, & Vologodskii A (2001). Dynamics of site juxtaposition in supercoiled DNA. Proceedings of the National Academy of Sciences of the United States of America, 98(3), 968–973. 10.1073/pnas.98.3.968 [PubMed: 11158579]

Incerti S, Baldacchino G, Bernal M, Capra R, Champion C, Francis Z, … Zacharatou C (2010). THE Geant4-DNA project. International Journal of Modeling, Simulation, and Scientific Computing, 1(2), 157–178. 10.1142/S1793962310000122

Incerti S, Ivanchenko A, Karamitros M, Mantero A, Moretto P, Tran HN, … Zacharatou C (2010). Comparison of GEANT4 very low energy cross section models with experimental data in water. Medical Physics, 37(9), 4692–4708. 10.1118/1.3476457 [PubMed: 20964188]

Incerti S, Kyriakou I, Bernal MA, Bordage MC, Francis Z, Guatelli S, … Brown JMC (2018). Geant4-DNA example applications for track structure simulations in liquid water: A report from the Geant4-DNA Project. Medical Physics, 0(0), 1–18. 10.1002/mp.13048

Karamitros M, Luan S, Bernal MA, Allison J, Baldacchino G, Davidkova M, … Incerti S (2014). Diffusion-controlled reactions modeling in Geant4-DNA. Journal of Computational Physics, 274, 841–882. 10.1016/j.jcp.2014.06.011

Karamitros Mathieu, Mantero A, Incerti S, Friedland W, Baldacchino G, Barberet P, … Zacharatou C (2011). Modeling Radiation Chemistry in the Geant4 Toolkit. Progress in Nuclear Science and Technology, 2(0), 503–508. 10.15669/pnst.2.503

Kassis AI, Harapanhalli RS, & Adelstein SJ (1999a). Comparison of strand breaks in plasmid DNA after positional changes of Auger electron-emitting iodine-125. Radiation Research, 151(2), 167–176. 10.2307/3579767 [PubMed: 9952301]

Kassis AI, Harapanhalli RS, & Adelstein SJ (1999b). Strand breaks in plasmid DNA after positional changes of auger electron- emitting iodine-125: Direct compared to indirect effects. Radiation Research, 152(5), 530–538. 10.2307/3580150 [PubMed: 10521930]

Klenin K, & Langowski J (2000). Computation of writhe in modeling of supercoiled DNA. Biopolymers, 54(5), 307–317. 10.1002/1097-0282(20001015)54:5<307::AID-BIP20>3.0.CO;2-Y [PubMed: 10935971]

Klimczak U, Ludwig DC, Mark F, Rettberg P, & Schulte-Frohlinde D (1993). Irradiation of plasmid and phage DNA in water-alcohol mixtures: Strand breaks and lethal damage as a function of scavenger concentration. International Journal of Radiation Biology, 64(5), 497–510. 10.1080/09553009314551711 [PubMed: 7902389]

Lampe N, Karamitros M, Breton V, Brown JMC, Kyriakou I, Sakata D, … Incerti S (2018). Mechanistic DNA damage simulations in Geant4-DNA part 1: A parameter study in a simplified geometry. Physica Medica, 48(February), 135–145. 10.1016/j.ejmp.2018.02.011 [PubMed: 29628360]

Lampe N, Karamitros M, Breton V, Brown JMC, Sakata D, Sarramia D, & Incerti S (2018). Mechanistic DNA damage simulations in Geant4-DNA Part 2: Electron and proton damage in a bacterial cell. Physica Medica, 48(June), 146–155. 10.1016/j.ejmp.2017.12.008 [PubMed: 29371062]

Leenhouts HP, & Chadwick KH (1985). Radiation Energy Deposition In Water Calculation of DNA Damage and Its Association with RBE. Radiation Protection Dosimetry, 13(1–4), 267–270.

Meesungnoen J, Benrahmoune M, Filali-Mouhim A, Mankhetkorn S, & Jay-Gerin J-P (2001). Monte Carlo Calculation of the Primary Radical and Molecular Yields of Liquid Water Radiolysis in the Linear Energy Transfer Range 0.3–6.5 keV/?m: Application to 137 Cs Gamma Rays1. Radiation Research, 155, 269–278. 10.1667/0033-7587(2001)155[0269:mccotp]2.0.co;2 [PubMed: 11175661]

Meylan S, Vimont U, Incerti S, Clairand I, & Villagrasa C (2016). Geant4-DNA simulations using complex DNA geometries generated by the DnaFabric tool. Computer Physics Communications, 204, 159–169. 10.1016/j.cpc.2016.02.019

Meylan Sylvain, Incerti S, Karamitros M, Tang N, Bueno M, Clairand I, & Villagrasa C (2017). Simulation of early DNA damage after the irradiation of a fibroblast cell nucleus using Geant4-DNA. Scientific Reports, 7(1), 1–15. 10.1038/s41598-017-11851-4 [PubMed: 28127051]

Milligan JR, Aguilera JA, & Ward JF (1993). Variation of single-strand break yield with scavenger concentration for plasmid DNA irradiated in aqueous solution. Radiation Research, 133(2), 151–157. 10.2307/3578350 [PubMed: 8382368]

Milligan JR, Arnold AD, & Ward JF (1992). The effect of superhelical density on the yield of single-strand breaks in γ-irradiated plasmid DNA. Radiation Research, 132(1), 69–73. 10.2307/3578335 [PubMed: 1410276]

Milligan JR, Wu CCL, Ng JY-Y, Aguilera JA, & Ward JF (1996). Characterization of the Reaction Rate Coefficient of DNA with the Hydroxyl Radical. Radiation Research, 146(5), 510. 10.2307/3579551 [PubMed: 8896577]

Nelder JA, & Mead R (1965). A Simplex Method for Function Minimization. The Computer Journal, 7(4), 308–313. 10.1093/comjnl/7.4.308

Nikjoo H, Uehara S, Willson WE, Hoshi M, & Goodhead DT (1998). Track structure in radiation biology: theory and applications. International Journal of Radiation Biology, 73(4), 355–

364. Retrieved from http://informahealthcare.com/doi/abs/10.1080/095530098142176 [PubMed: 9587072]

Patrick Higgins N, & Vologodskii AV (2015). Topological Behavior of Plasmid DNA. Plasmids, 3(2), 105–131. 10.1128/9781555818982.ch7

Perl J, Shin J, Schümann J, Faddegon B, & Paganetti H (2012). TOPAS: An innovative proton Monte Carlo platform for research and clinical applications. Medical Physics, 39(11), 6818–6837. 10.1118/1.4758060 [PubMed: 23127075]

Perry CC, Ramos-Méndez J, & Milligan JR (2020). DNA condensation with a boron-containing cationic peptide for modeling boron neutron capture therapy. Radiation Physics and Chemistry, 166(September 2019), 108521. 10.1016/j.radphyschem.2019.108521 [PubMed: 32454570]

Peukert C, Incerti S, Kempson I, Douglass M, Karamitros M, Baldacchino G and Bezak E (2019) Validation and investigation of reactive species yields of Geant4-DNA chemistry models Medical Physics (46):983–98. 10.1002/mp.13332 [PubMed: 30536689]

Pimblott SM, & Green NJB (1992). Stochastic modeling of partially diffusion-controlled reactions in spur kinetics. Journal of Physical Chemistry, 96(23), 9338–9348. 10.1021/j100202a052

Pimblott SM, & LaVerne JA (1997). Stochastic simulation of the electron radiolysis of water and aqueous solutions. Journal of Physical Chemistry A, 101(33), 5828–5838. 10.1021/jp970637d

Plante I (2011). A Monte-Carlo step-by-step simulation code of the non-homogeneous chemistry of the radiolysis of water and aqueous solutions. Part I: Theoretical framework and implementation. Radiation and Environmental Biophysics, 50(3), 389–403. 10.1007/s00411-011-0367-8 [PubMed: 21562854]

Ramos-Méndez J, Domínguez-Kondo N, Schuemann J, McNamara A, Moreno-Barbosa E, & Faddegon B (2020). LET-dependent intertrack yields in proton irradiation at ultra-high dose rates relevant for FLASH therapy. Radiation Research, 194(4), 351–362. 10.1667/RADE-20-00084.1 [PubMed: 32857855]

Ramos-Méndez J, Perl J, Schuemann J, McNamara A, Paganetti H, & Faddegon B (2018). Monte Carlo simulation of chemistry following radiolysis with TOPAS-nBio. Physics in Medicine and Biology, 63(10), 0–12. 10.1088/1361-6560/aac04c

Ramos-Méndez José, Shin WG, Karamitros M, Domínguez-Kondo J, Tran NH, Incerti S, … Faddegon B (2020). Independent reaction times method in Geant4-DNA: Implementation and performance. Medical Physics. 10.1002/mp.14490

Sakata D, Belov O, Bordage MC, Emfietzoglou D, Guatelli S, Inaniwa T, … Incerti S (2020). Fully integrated Monte Carlo simulation for evaluating radiation induced DNA damage and subsequent repair using Geant4-DNA. Scientific Reports, 10(1), 1–13. 10.1038/s41598-020-75982-x [PubMed: 31913322]

Sakata D, Lampe N, Karamitros M, Kyriakou I, Belov O, Bernal MA, … Incerti S (2019). Evaluation of early radiation DNA damage in a fractal cell nucleus model using Geant4-DNA. Physica Medica, 62(January), 152–157. 10.1016/j.ejmp.2019.04.010 [PubMed: 31109825]

Shin W-G, Ramos-Mendez J, Hoang Ngoc T, Perrot Y, Incerti S, Okada S, & Villagrasa C (2021). Geant4-DNA simulation of the pre-chemical stage of water radiolysis and its impact on initial radiochemical yields. Physica Medica, 88(77), 86–90. [PubMed: 34198026]

Shin WG, Ramos-Mendez J, Faddegon B, Tran HN, Villagrasa C, Perrot Y, … Incerti S (2019). Evaluation of the influence of physical and chemical parameters on water radiolysis simulations under MeV electron irradiation using Geant4-DNA. Journal of Applied Physics, 126(11). 10.1063/1.5107511

Takata H, Hanafusa T, Mori T, Shimura M, Iida Y, Ishikawa K, … Maeshima K (2013). Chromatin Compaction Protects Genomic DNA from Radiation Damage. PLoS ONE, 8(10), 1–11. 10.1371/journal.pone.0075622

Toburen L (2014). Development of Monte Carlo Track Structure Codes. Nasa, 2–6. Retrieved from https://three.jsc.nasa.gov/articles/Monte-Carlo-Track-Structure-Toburen.pdf

Tomita H, Kai M, Kusama T, & Ito A (1998). Monte Carlo simulation of DNA strand-break induction in supercoiled plasmid pBR322 DNA from indirect effects. Radiation and Environmental Biophysics, 36(4), 235–241. 10.1007/s004110050077 [PubMed: 9523339]

Tomita Hiroyuki, Kai Y, & Kusama AT (1995). Strand Break Formation in Plasmid DNA Irradiated in Aqueous Solution: Effect of Medium Temperature and Hydroxyl Radical Scavenger Concentration. Radiat. Res, 36, 46–55.

Turner JE, Magee JL, & Wright HA (1983). Physical and chemical development of electron tracks in liquid water. Radiation Research, 96(3), 437–449. 10.2307/3576111

Vologodskii AV, & Nicholas CR (1994). Conformational And Thermodynamic Properties of Supercoiled DNA. Annu. Rev. Biophys. Struct, (23).

Vyšín L, Pachnerová Brabcová K, Štěpán V, Moretto-Capelle P, Bugler B, Legube G, … Davídková M (2015). Proton-induced direct and indirect damage of plasmid DNA. Radiation and Environmental Biophysics, 54(3), 343–352. 10.1007/s00411-015-0605-6 [PubMed: 26007308]

Watanabe R, Rahmanian S, & Nikjoo H (2015). Spectrum of Radiation-Induced Clustered Non-DSB Damage - A Monte Carlo Track Structure Modeling and Calculations. Radiation Research, 183(5), 525–540. 10.1667/RR13902.1 [PubMed: 25909147]

Wright HA, Magee JL, Hamm RN, Chatterjee A, Turner JE, & Klots CE (1985). Calculations of Physical And Chemical Reactions Produced in Irradiated Water Containing DNA. Radiation Protection Dosimetry, 13(1–4), 133–136.

Zaider M, Brenner DJ, & Wilson WE (1983). The applications of track calculations to radiobiology I. Monte Carlo simulation of proton tracks. Radiation Research, 95(2), 231–247. 10.2307/3576252

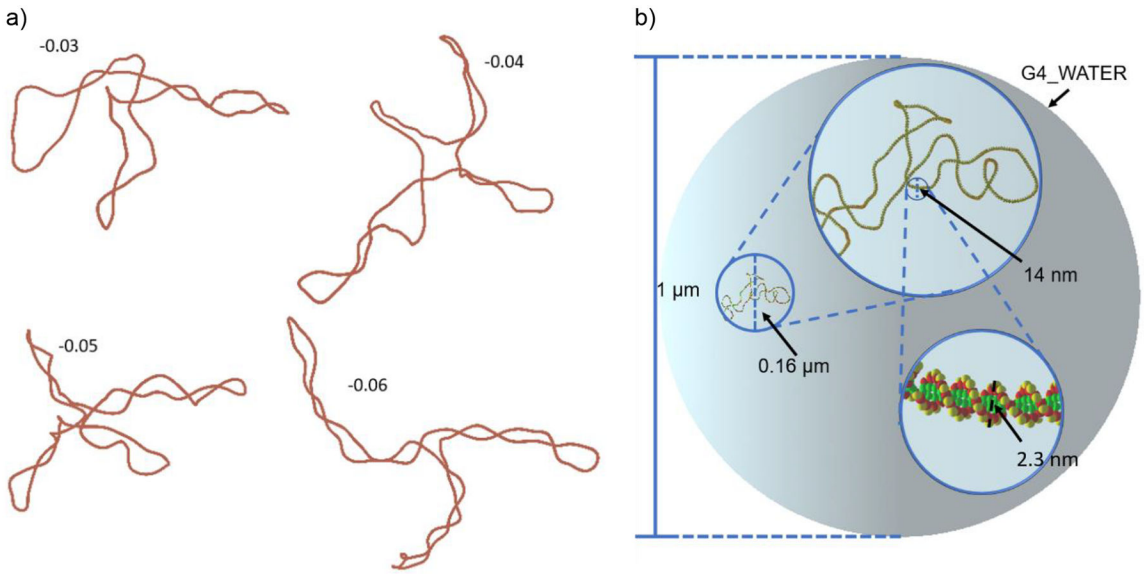

Figure 1: Plasmid DNA geometries used in Geant4-DNA.

a) Examples of four pUC19 plasmids generated with a σ ranging from −0.03 to −0.06 used to calculate the DNA geometry for both direct and indirect DNA damage. b) Basic simulation geometry setup illustrating the use of plasmid skeletons to wrap the simple DNA model used in this work. The coordinate positions of DNA components for radiation chemistry simulation were located at the center of the semi-spheres.

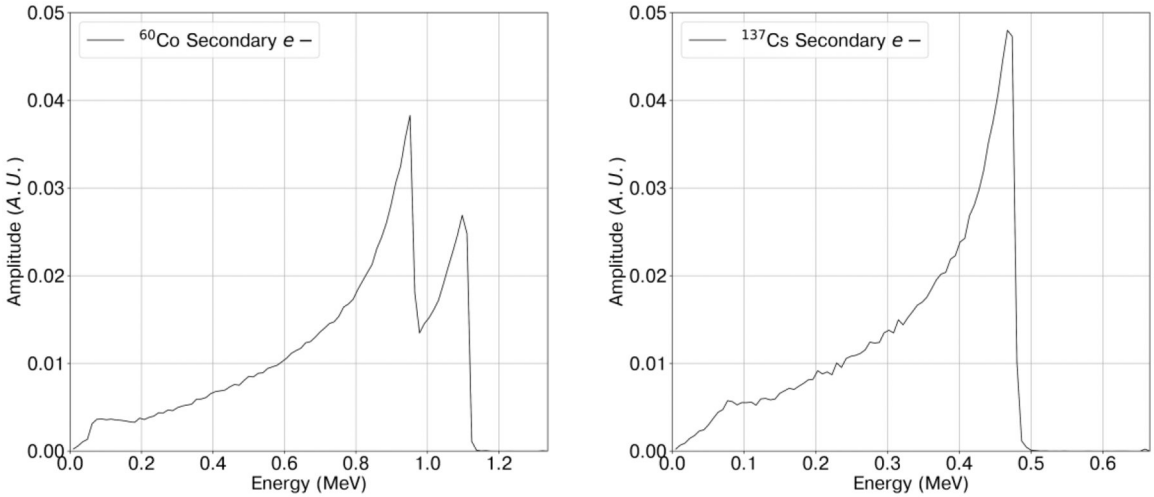

Figure 2: Secondary electron spectrum for ^{60}Co and ^{137}Cs.

Energy spectrums were calculated using condensed history MC using TOPAS.

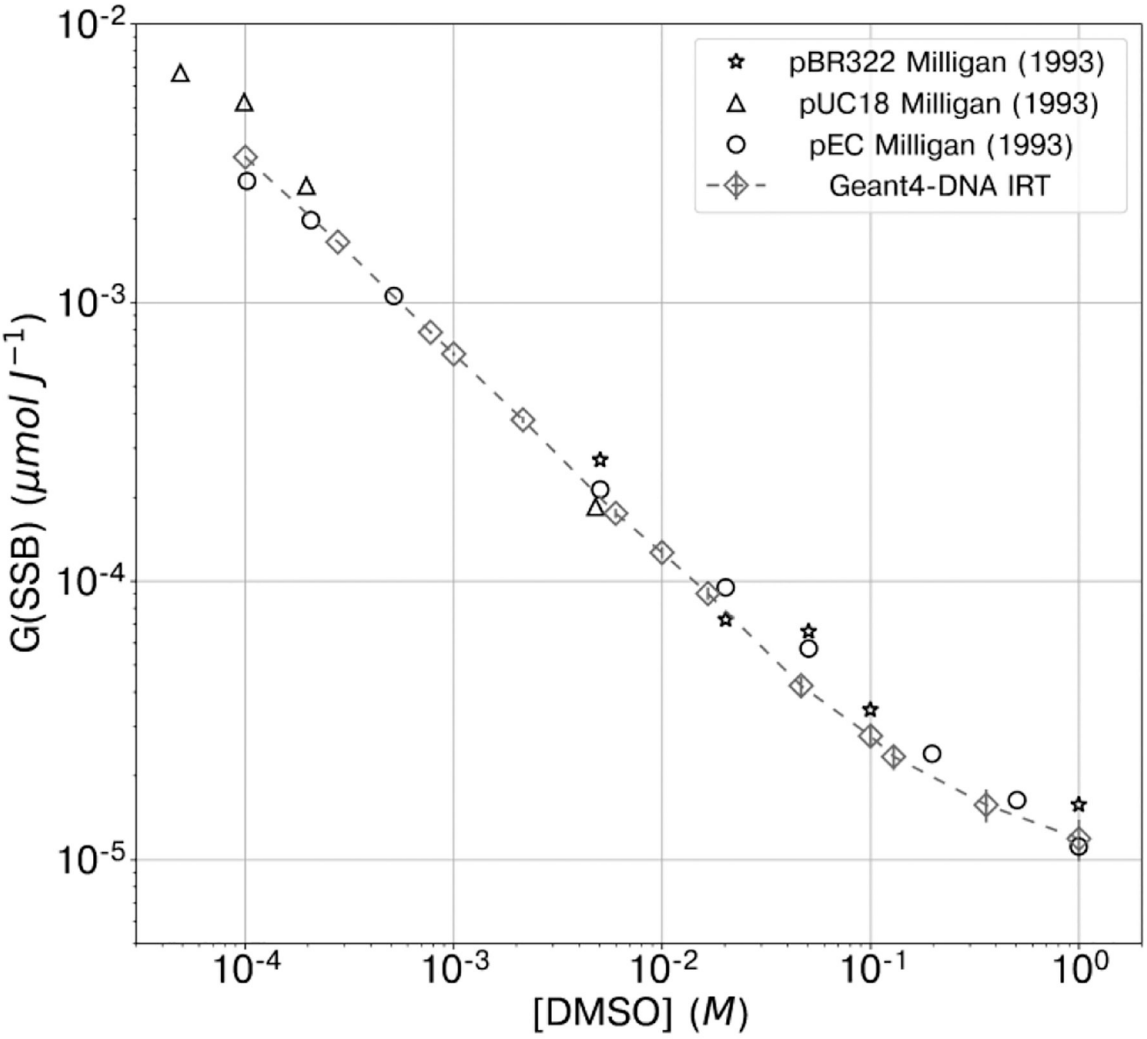

Figure 3: S1) Response of G(SSB) (μmol J^{-1}) to [DMSO].

Error bars represent statistical uncertainties, one standard deviation. Geant4-DNA IRT results (gray ◇), reference experimental data from Milligan et al., (1993) corresponds to pBR322 (☆), pUC18 (△), and pEC (○) plasmids.

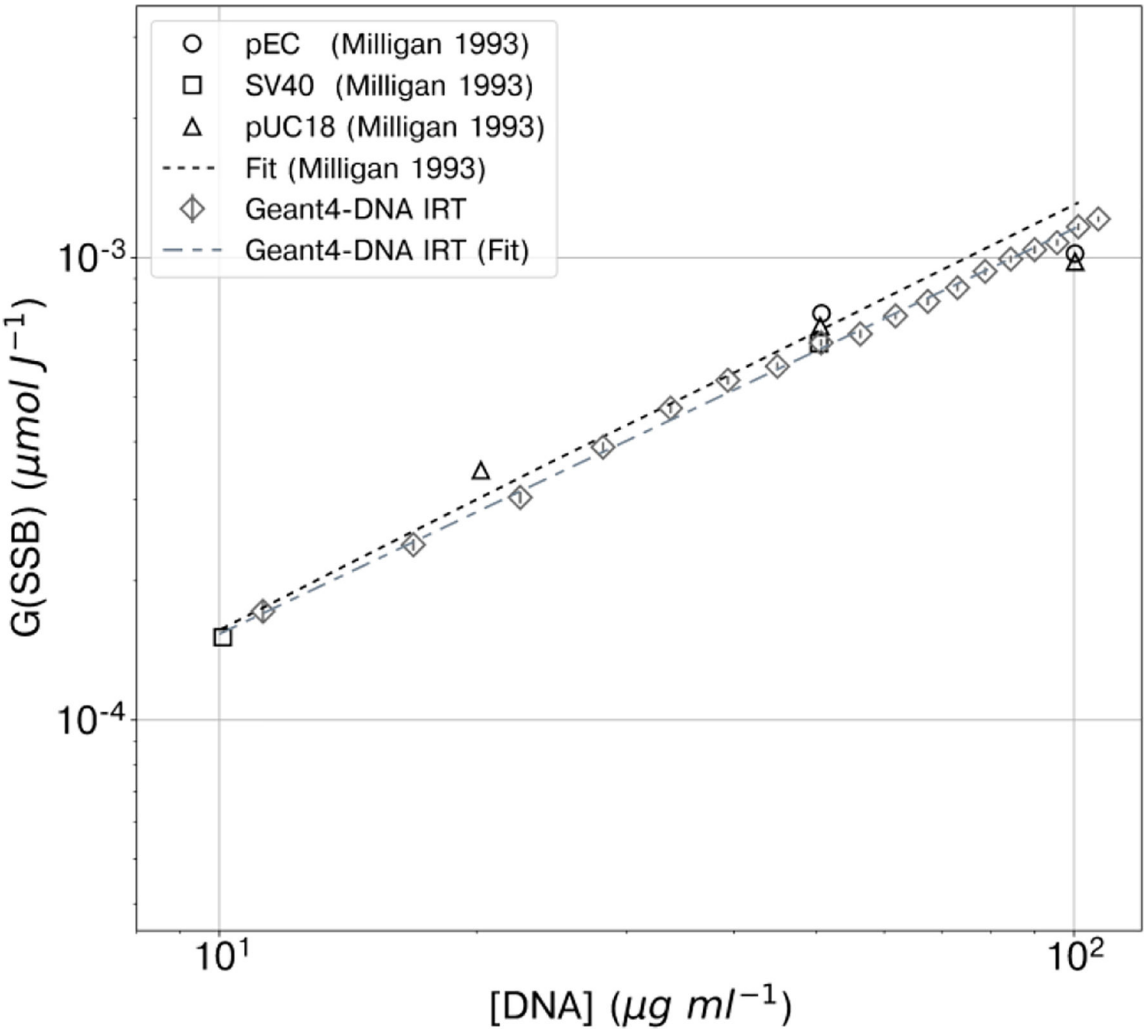

Figure 4: [DNA] (μg/mL) response of G(SSB) (μmol J^{-1}).

Error bars represent statistical errors, one standard deviation. Geant4-DNA IRT results are shown (◇), experimental data are from Milligan, 1993 (○, □, △).

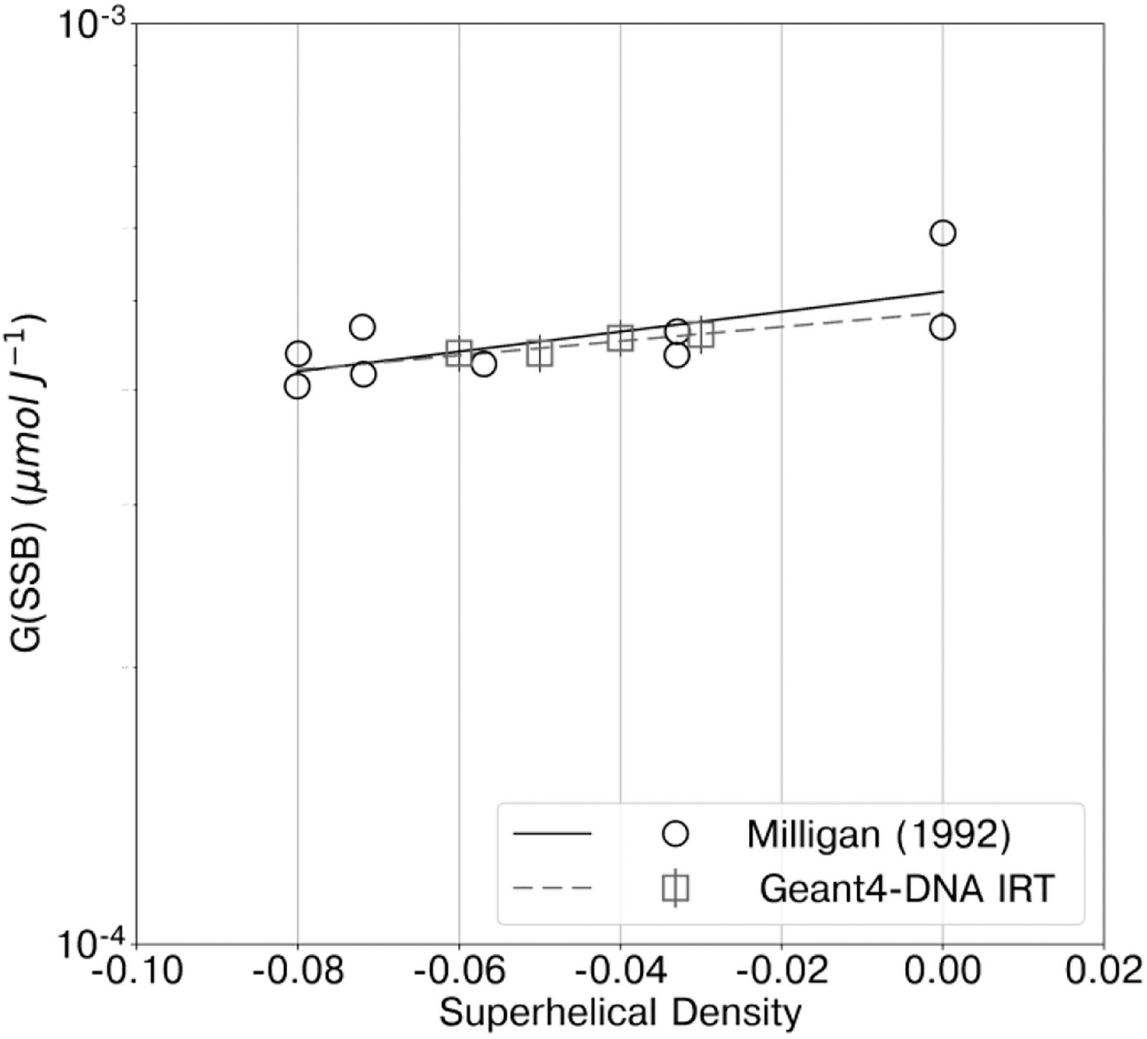

Figure 5: Response of G(SSB) (μmol J^{-1}) to σ.

Error bars represent statistical errors, one standard deviation. Geant4-DNA IRT results (□), experimental data from Milligan et. al. (1992) is shown (○) with a correspondent fit. Both, the experimental (solid line) data and simulation (dashed line) were fitted using a double logarithmic function to better represent their behaviors

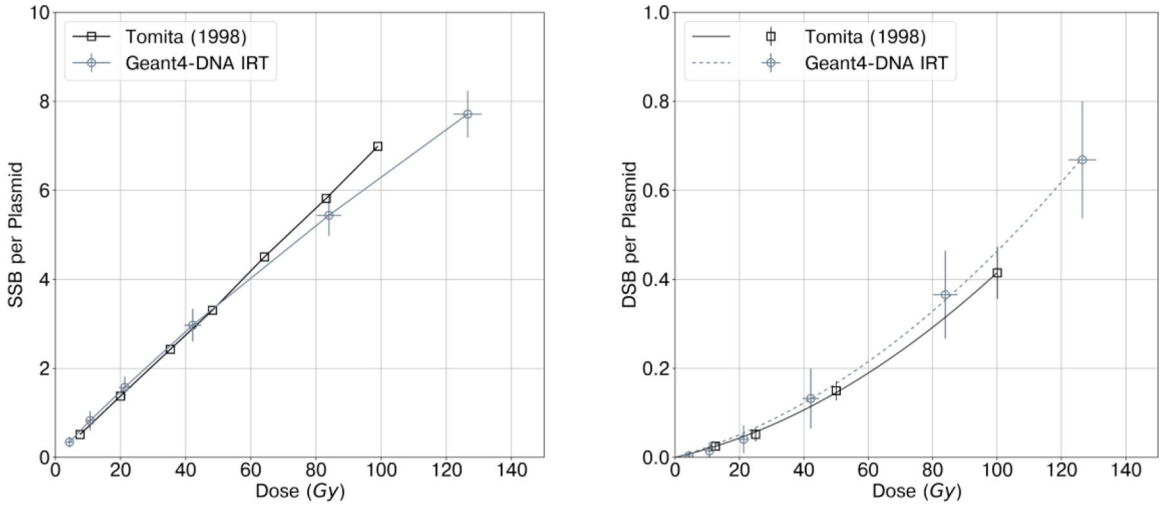

Figure 6: Dose response of SSB (left), and DSB (right).

Error bars represent one standard deviation. Simulation results for SSB and DSB (○) are shown alongside Tomita's (1998) reference data (□). Simulation data 2nd order polynomial fit is shown with the dotted line.

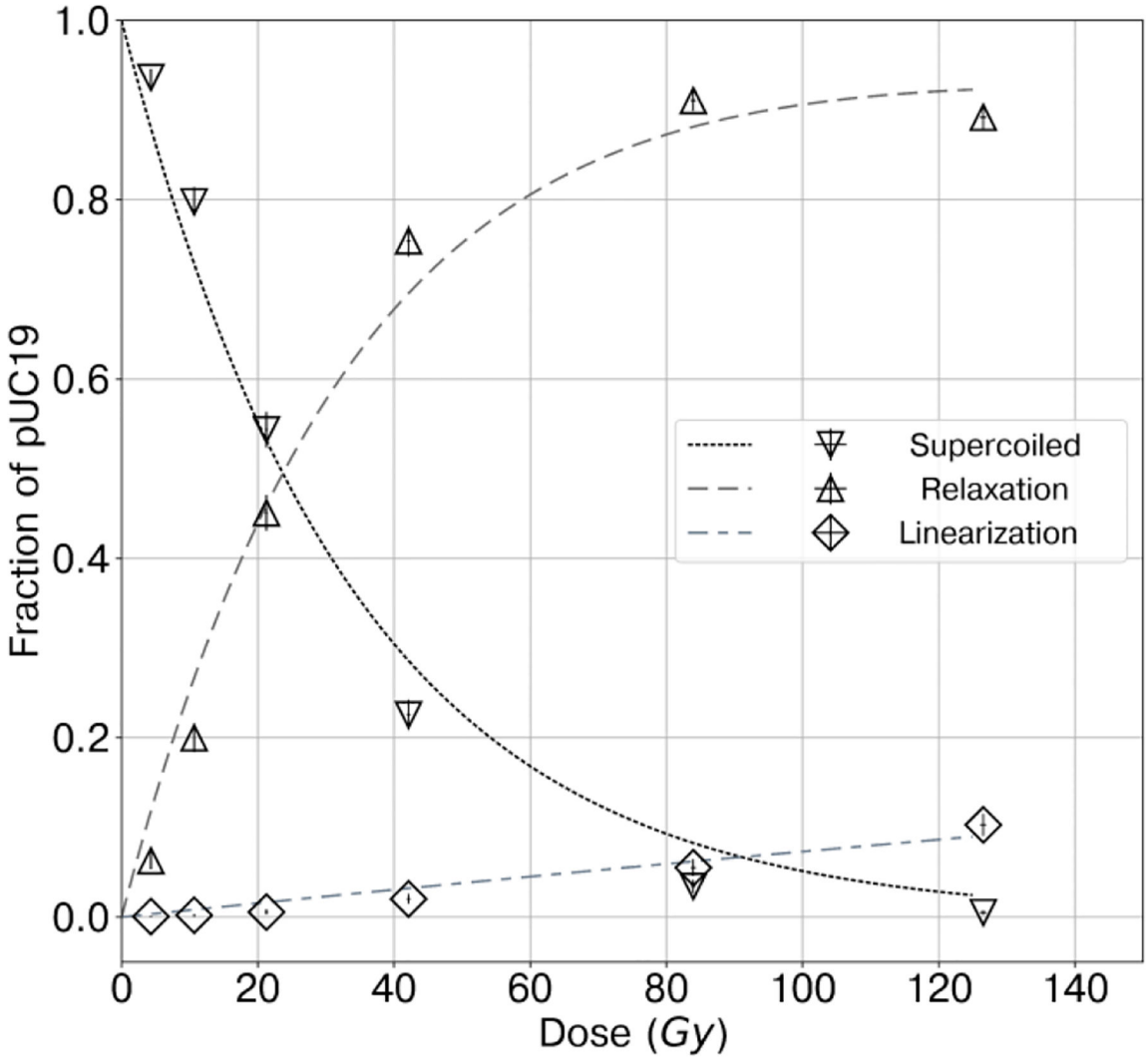

Figure 7: Fraction of pUC19.

Error bars represent statistical uncertainty, one standard deviation. Results separated in supercoiled (▽), relaxed (△) and linearized fractions (◇) fitted to the Cowan (1987) model and.

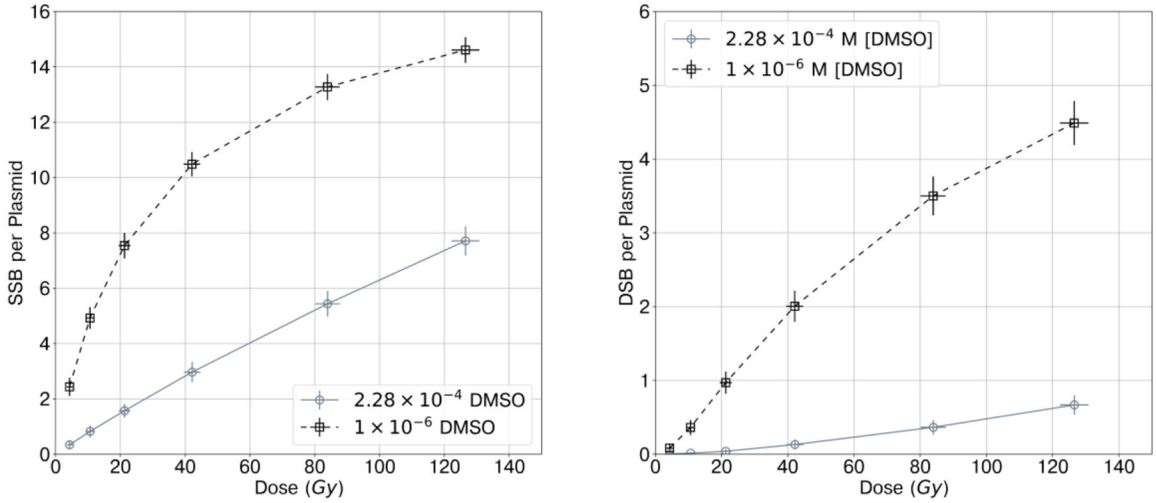

Figure 8: DMSO effect on SSB and DSB as dose increases.

Error bars represent one standard deviation. 1×10^{-6} M [DMSO] is shown (□) against 2.28×10^{-4} M [DMSO] (○), from MCTS simulations with pUC19 plasmids.

Table 1:

List of chemical reactions used in this work with Geant4-DNA IRT to perform DNA damage simulations.

Reactions involving O_2 were treated as pseudo-first-order. Products from reactions with DMSO were not included. 1 M = 1 mole dm^{-3}

Reactions for simulation of radiolysis in pure liquid water		
No.	**Reaction**	**k_{obs} ($M^{-1}s^{-1}$)**
1	$e_{aq}^{-1} + {}^{\bullet}OH \rightarrow OH^-$	2.95×10^{10}
2	$e_{aq}^{-1} + H_2O_2 \rightarrow OH^- + {}^{\bullet}OH$	1.10×10^{10}
3	${}^{\bullet}OH + H^{\bullet} \rightarrow H_2O$	1.55×10^{10}
4	$H^{\bullet} + H_2O_2 \rightarrow {}^{\bullet}OH + H_2O$	9.00×10^{7}
5	${}^{\bullet}OH + {}^{\bullet}OH \rightarrow H_2O_2$	5.50×10^{9}
6	$e_{aq}^{-1} + e_{aq}^{-1} \rightarrow H_2 + OH^-$	6.36×10^{9}
7	$H_3O^+ + OH^- \rightarrow 2H_2O$	1.13×10^{11}
8	$e_{aq}^{-1} + H_3O^+ \rightarrow H^{\bullet} + H_2O$	2.11×10^{10}
9	$e_{aq}^{-1} + H^{\bullet} \rightarrow OH^- + H_2$	2.50×10^{10}
10	$H^{\bullet} + H^{\bullet} \rightarrow OH^- + H_2$	5.03×10^{10}
TRIS and EDTA		
No.	Reaction	k_{obs} ($M^{-1}s^{-1}$)
20	EDTA + OH	1.5×10^{9}
21	TRIS + OH	1.2×10^{9}

DNA damage reactions		
No.	**Reaction**	**k_{obs} ($M^{-1}s^{-1}$)**
11	${}^{\bullet}OH + DNA \rightarrow OHDNA$	Equation 1
12	$H^{\bullet} + DNA \rightarrow HDNA$	3.00×10^{7}
13	$e_{aq}^{-1} + DNA$	1.00×10^{7}
Oxygen Reactions		
No.	Reaction	k_{obs} ($M^{-1}s^{-1}$)
14	$e_{aq}^{-1} + O_2 \rightarrow O_2^-$	1.90×10^{10}
15	$H^{\bullet} + O_2 \rightarrow HO_2$	2.10×10^{10}
16	${}^{\bullet}OH + HO_2 \rightarrow O_2 + H_2O$	7.90×10^{9}
DMSO		
No.	Reaction	k_{obs} ($M^{-1}s^{-1}$)
17	${}^{\bullet}OH + DMSO$	7.10×10^{9}
18	$H^{\bullet} + DMSO$	2.70×10^{7}
19	$e_{aq}^{-1} + DMSO$	3.80×10^{6}

Table 2:

Parameters of the simulation setups;

The scenarios were set to determine the dependence of SSB on DMSO concentration (S1), DNA concentration (S2), pUC19 superhelix density (S3), and for SSB and DSB on absorbed dose (S4). Each scenario was configured to recreate the experimental conditions of their respective references.

Scenario	Dose (Gy)	[DNA] (μg/mL)	[DMSO] (M)	σ	$[O_2]$ (mM)	Source	Reference
S1	30	50.6	10^{-4} – 1	−0.03	0.27	^{137}Cs	Milligan et al., 1993
S2	30	5.62 – 100.12	1.00×10^{-3}	−0.03	0.27	^{137}Cs	Milligan et al., 1993,1996
S3	80	50.6	4.56×10^{-3}	−0.06 – −0.03	0.27	^{137}Cs	Milligan et al., 1992
S4	0 – 120	33.73	2.28×10^{-4}	−0.03	0.27	^{60}Co	Tomita et al., 1998

Table 3:

Direct DNA damage against DNA concentration for ^{60}Co and ^{137}Cs γ sources respectively.

Results are shown alongside their statistical uncertainties, one standard deviation.

[DNA] (μg mL^{-1})	^{60}Co SSB (μmol J^{-1})	^{137}Cs SSB (μmol J^{-1})
5.62	$3.58\times10^{-8} \pm 1.0\times10^{-8}$	$3.11\times10^{-8} \pm 7.7\times10^{-9}$
11.24	$7.20\times10^{-8} \pm 1.45\times10^{-8}$	$6.21\times10^{-8} \pm 1.1\times10^{-8}$
16.86	$9.89\times10^{-8} \pm 1.74\times10^{-8}$	$1.06\times10^{-7} \pm 1.45\times10^{-8}$
22.48	$1.47\times10^{-7} \pm 2.1\times10^{-8}$	$1.28\times10^{-7} \pm 1.6\times10^{-8}$
28.1	$1.59\times10^{-7} \pm 1.8\times10^{-8}$	$1.74\times10^{-7} \pm 2.4\times10^{-8}$
33.72	$2.18\times10^{-7} \pm 2.6\times10^{-8}$	$1.92\times10^{-7} \pm 1.9\times10^{-8}$